Accuracy and Survivability of Distributed Fiber Optic Temperature Sensors

Nur Aida Abdul Rahim[1], Matthew A. Davis[2], Luke Routhier[3], Baohe Chang[4], Jason Chevalier[5], Joseph J. Bos[6], Stephen T. Kreger[7], Eric E. Sanborn[8]

Luna Innovations Inc., 3157 State Street, Blacksburg, VA 24060

Obtaining a high accuracy, high spatial resolution temperature profile of critical test artifacts and test components has long been the holy grail of temperature sensing. Optical Frequency-Domain Reflectometry (OFDR) facilitates the use of unaltered optical fiber as high resolution distributed temperature sensors. Coating selection is a major parameter to consider in determining the best sensor choice based on the operating environment, especially the temperature range. We assess the performance of several fiber sensor coatings for the purpose of converging to the best sensor option for the -40°C to 200°C range. Stripped and carbon coated fiber maintain uniformity through the temperature cycles, resulting in accuracies of +/-0.5°C. A packaged fiber sensor was also held at 551°C for 3000 hrs to measure its performance over time. The survivability and accuracy of fiber sensors at high temperatures provide clear advantages compared to single point thermocouples in terms of displaying localized temperature variations.

Nomenclature

EMI	=	Electromagnetic Interference
LBL	=	Low Bend Loss
OBR	=	Optical Backscatter Reflectometer
OD	=	Outer diameter
ODiSI	=	Optical Distributed Sensor Interrogator
OFDR	=	Optical Frequency-Domain Reflectometry
PS	=	Pure Silica
RBS	=	Rayleigh Backscatter
RTD	=	Resistance Temperature Detectors
SMF	=	Single Mode Fiber

I. Introduction

Optical fiber sensors provide numerous advantages for space, air and ground sensing applications. They are small, light-weight, immune to EMI, radiation resistant, and can be embedded in a material or adhered to its surface. These factors make optical fiber ideal for aerospace measurement applications in which weight and non-intrusiveness are key.

In this work, recent advancements in Optical Frequency Domain Reflectometry (OFDR)-based optical fiber temperature sensing are demonstrated. Utilizing Rayleigh backscatter (RBS) from off-the-shelf single mode fiber as the transducer, OFDR technology enables low-cost, fully-distributed sensing with millimeter spatial resolution and high dynamic range[1, 2]. The ability to obtain temperature measurements at a high spatial density results in the ability

---

[1] Field Applications Engineer, Lightwave Division, 3157 State Street.
[2] Team Lead - Harsh Environment Sensing, Lightwave Division, 3157 State Street, AIAA Member.
[3] Student Co-op, Lightwave Division, 3157 State Street.
[4] Materials Research Engineer, Lightwave Division, 3157 State Street.
[5] Engineer, Lightwave Division, 3157 State Street.
[6] Senior Development Engineer, Gentex Corporation, MI.
[7] Senior Optical Engineer, Lightwave Division, 3157 State Street.
[8] Senior Mechanical Engineer, Intuitive Surgical, 1715 Pratt Drive, Suite 3600.

to then view the temperature profile across a whole test artifact as opposed to obtaining measurements at discrete locations. One is then able to better assess parameters important to a test, such as hot spot locations and temperature uniformity, which influence output efficiency[3, 4, 5].

Optical fibers are manufactured with a variety of coatings, ranging from polymers (polyimide, Ormocer, acrylate) to metals (gold, copper, aluminum). This results in a slew of options for selecting a fiber type best suited for distributed temperature measurements. We evaluate measurement accuracies of seven fiber types within the -40°C to 200°C range in a controlled environment. Based on these results, a packaged sensor was built and tested in a furnace at higher temperatures.

The sensors described here enable more accurate wind tunnel and ground based testing at a reduced cost. They are also shown here to survive the timescales needed for future flight consideration as a measurement device for high temperature applications such as those that surround the engine.

II.   Measurement Theory

The temperature sensor is formed by standard off-the-shelf optical fiber composed of a monolithic fused silica core and cladding and a protective coating which is typically composed of a polymer or metal. An individual sensing fiber can be many meters in length and provide thousands of strain measurements at points distributed along its length. Measurements are made using the Rayleigh scatter in the fiber, a random but stable pattern of reflections inherent to each fiber as a result of small-scale non-homogeneities in the fiber, such as glass composition fluctuations. This random pattern of reflections is unique to each fiber and constant for the life of the fiber, forming a reflection 'fingerprint'. Temperature changes experienced by the sensor results in variations of both its refractive index (due to the thermo-optic coefficient, *dn/dT*) and its length (due to the coefficient of thermal expansion, CTE). Both these effects result in an apparent stretching of this 'fingerprint', which translates to a shift in the spectral content of the 'fingerprint'.

Sensors are interrogated using optical frequency domain reflectometry (OFDR), an interferometric technique which can distinguish sensors or scattering points at different locations along the fiber. Figure 1 describes the basic OFDR network. Light from a swept-tunable laser is split between the measurement path and a reference path by a fiber optic coupler. Light in the measurement path is sent to the sensing fiber through the input path of an optical coupler. Light reflected from the sensing fiber returns through the coupler and is recombined with light from the reference path. This combined signal then passes through a polarization beam splitter, which splits the light into orthogonal states recorded at the S and P detectors. A Fourier transform of these signals yields the phase and amplitude of the signal as a function of length along the fiber, i.e. the fiber 'fingerprint'.
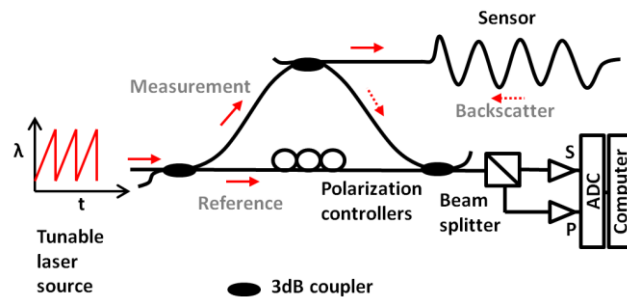
Figure 1. Basic OFDR optical network.

To calculate temperature change, the spectral content of the fiber's 'fingerprint' is compared between the measurement and reference state. Complex Fourier transform data is windowed around a desired measurement location (Figure 2A). This window length forms the gage length of the strain measurement. An inverse Fourier transform of the windowed data gives the spectral content from a particular gage in the sensing fiber (Figure 2B), which is cross-correlated (Figure 2C) with the spectrum from the same location of fiber in a baseline state. Finally, the cross-correlated shift is converted to temperature change using a calibration coefficient. This process is repeated along the length of the sensing region, forming a distributed measurement.
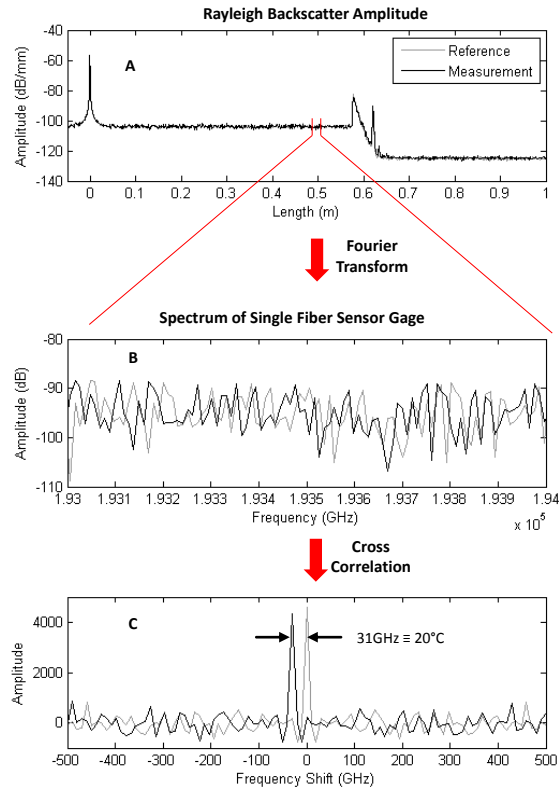
Figure 2. Frequency shift calculation from Rayleigh scatter measurement. A: Rayleigh backscatter along optical path. B: Spectrum of single fiber sensor gage. C: Cross-correlation of reference and measurement spectra.

American Institute of Aeronautics and Astronautics

III. Methods

A. Cyclic Test

1. Aluminum Enclosure

An enclosure was machined out of solid aluminum (Figure 3) to house the optical fibers during temperature testing. The mass of the enclosure ensured that the temperature distribution within the enclosure cavity was uniform throughout the test. Desiccant packs were used within the enclosure to limit humidity variation.
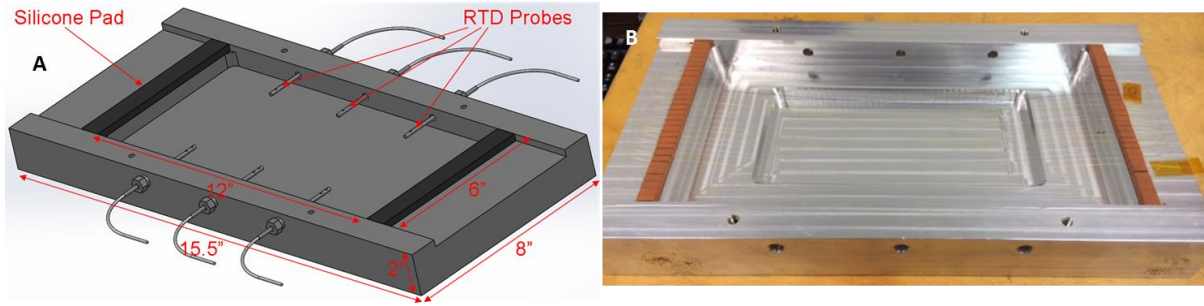
Figure 3. A: Aluminum enclosure. B: Fiber layout within enclosure.

Temperature uniformity within the enclosure cavity was verified in a pre-test with multiple fiber passes (Figure 4). A representative plot of frequency shift as a function of length along the sensor is seen to be uniform for each fiber type, confirming the temperature uniformity within the enclosure.
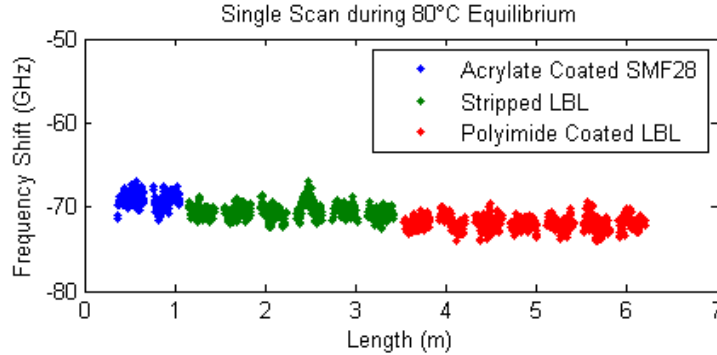
Figure 4. Frequency shift along acrylate coated, stripped, and polyimide coated sensor string, at 80°C during pre-test.

2. RTDs

Six calibrated Platinum RTDs (resistance temperature detectors) were used for these tests, as the temperature measurement standard against which the fiber measurements were compared. The RTDs were 4-wire, class 1/3B, wire wound (Omega). The manufacturer-specified accuracy for these RTDs is within the -50°C-250°C range. RTD tolerances were measured using a metrology well (Fluke, model 9144) from 50°C to 200°C. An Agilent 34972A electrical readout system was used to log RTD measurements.

3. Fiber Layout

A single fiber sensor was strung in multiple passes within the enclosure (Figure 5). The sensor consisted of multiple fiber types spliced together in the order shown in Table 1. Fiber types were arranged in order of increasing numerical aperture (NA). The carbon-coated fiber originally had an acrylate overcoat which was chemically

removed using acetone and the stripped LBL originally had a polyimide coating which was removed with sulfuric acid.
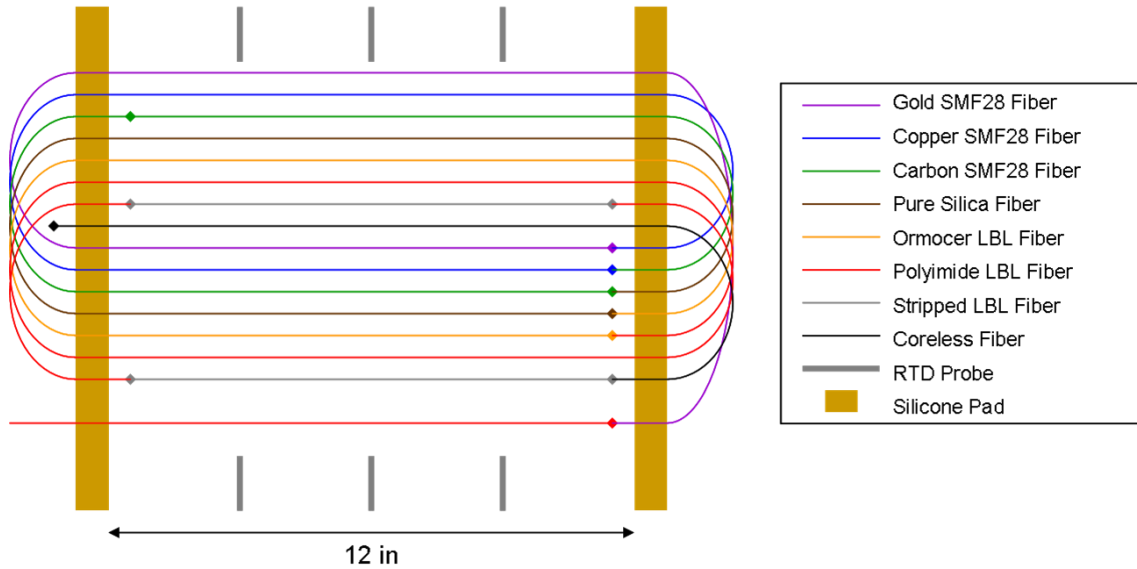
Figure 5. Fiber layout within aluminum enclosure.

Table 1. Fiber type order along sensor string.

Fiber Type	Coating	Numerical Aperture
SMF-28	Gold	0.12
SMF-28	Copper	0.13
SMF-28	Carbon	0.14
Pure Silica	Polyimide	0.17
SMF-LBL	Ormocer	0.20
SMF-LBL	Polyimide	0.21
SMF-LBL	None	0.21

Silicone pads were used to hold the fiber ingress and turnarounds. The fiber was instrumented loosely drooping between the silicone pad strips, without touching the bottom of the cavity. This droop was necessary to compensate for thermal expansion of the aluminum enclosure at maximum temperature, and effectively isolate the fiber from strain.

An aluminum lid was bolted on the enclosure before installation in a temperature chamber (Tenney model TJR).

4. Temperature Profile

The temperature chamber was programmed to cover the temperature range of -40°C - 200°C at a ramp rate of 5°C per hour with 5 hour dwells at the temperature limits. This ramp rate was previously determined to be sufficiently slow to allow the enclosure to be in equilibrium throughout the test. This temperature cycle was run five times. Frequency shift (fiber) and temperature (RTD) measurements were recorded once a minute. Fiber data was collected using Luna's ODiSI B system. The ODiSI B was used in the Standard Configuration, with a 100 Hz base acquisition rate, 5 mm gage length and 2.5 mm sensor spacing.

B. High Temperature Test

A stripped fiber sensor configuration was selected for the high temperature test. In order to ensure the durability of the stripped sensor, it was housed in a glass capillary inserted into a stainless steel tube. A packaged sensor from the test can be seen in Figure 6, along with a schematic of its cross section (not to scale). The fiber (OD 125µm) is much smaller than the glass capillary (OD 350 µm) which in turn is much smaller than the stainless steel tube (OD 1/16 inches), thus thermal expansion of the stainless steel tube does not transfer strain to the fiber. The matched CTE between the stripped fiber sensor and glass capillary would further ensure minimal expansion mismatch with temperature change.
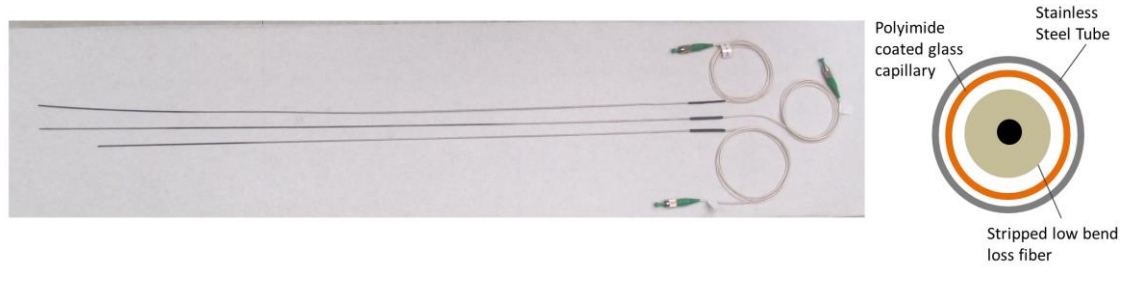
Figure 6. Packaged high temperature sensor and schematic of sensor cross section.

The sensor was placed into a small box furnace capable of 1000°C such that it passed through the furnace. In addition to the fiber optic sensor, 4 K-Type thermocouples were located at location L = 0.34 m, 0.46 m, 0.52 m, and 0.59 m along the fiber. The furnace temperature was increased such that the sensors were held steady at a temperature of ≈550°C. The furnace and experimental setup can be seen in Figure 7.Figure 7. Furnace and experimental setup for high temperature test. Data was sampled once per day with Luna's OBR system over the course of approximately 5 months for a cumulative exposure to these temperatures of more than 3600 hours. Based on equipment availability, there were periods in which data was not taken. Measurements were post processed with a gage length of 0.5 cm and a sensor spacing of 0.1 cm.
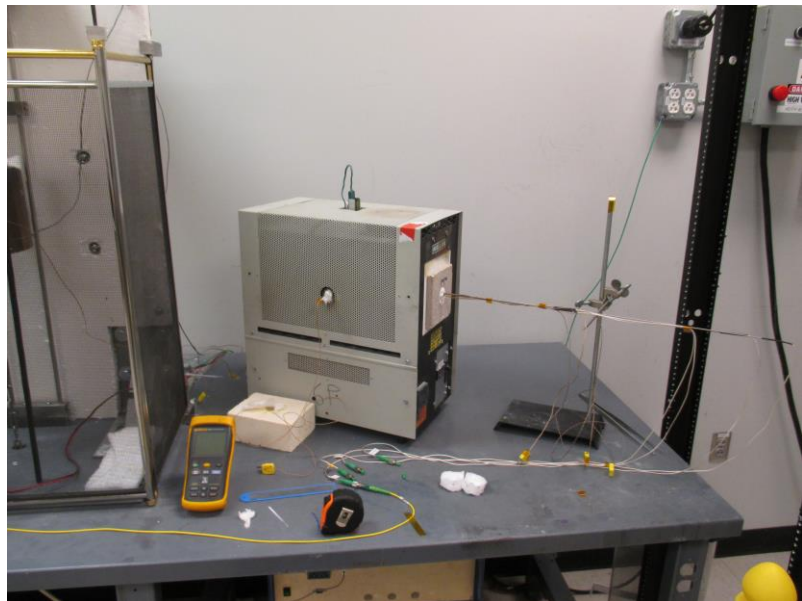
Figure 7. Furnace and experimental setup for high temperature test.

IV. Results and Discussion

A. Cyclic Test

A plot of relative frequency shift along the length of the sensor is shown in Figure 8 (relative to average shift). It is immediately obvious that the metal coated fibers experience large variations along the fiber length whereas

stripped and polymer-coated fibers display very consistent length-wise uniformity. This non-uniform lengthwise response has been repeatedly observed on metal coated fibers. It is theorized that a few factors might result in this behavior: it is possible that handling induces stresses in the coating that do not immediately relax; the coating may slip against the glass, creating non-uniform and time varying strains; non-uniformity in coating thickness could be a problem.
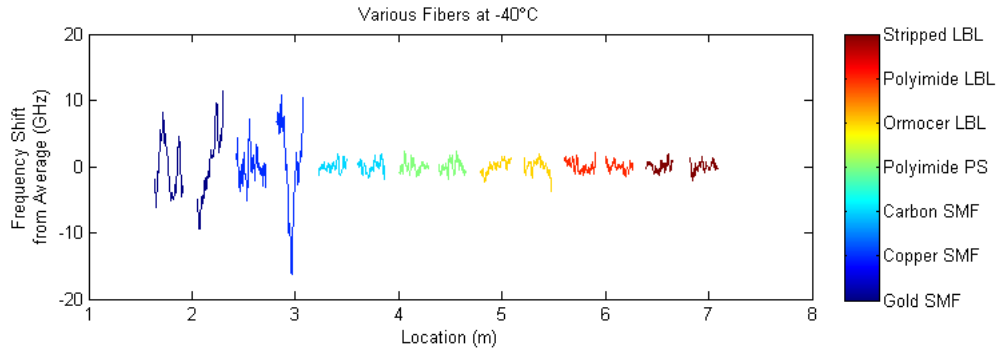
Figure 8. Frequency shift along the length of the sensor string, for all fiber types (color-coded).

The fiber was cycled through the -40°C - 200°C range at a ramp rate of 5°C per hour with 5 hour dwells at the temperature limits. Measurements of fiber frequency shift against RTD temperature were fit with both a linear and 4th order polynomial (quartic) fit using Matlab's *polyfit* function, in order to obtain temperature coefficients for each fiber type. The first two cycles were considered to be exercise cycles, required to relax the polymer coatings on both the polyimide- and Ormocer-coated fibers. For cycles 3 through 5, frequency shift values from the fiber sensor were obtained by averaging the frequency shift along all fiber segments of a specific type in the central 25cm of the enclosure. All 6 RTD measurements were averaged to obtain absolute temperature measurements. RTD measurements remained within 1°C of each other throughout the test. Plots of frequency shift against RTD temperature measurements are shown in the first row of Figure 9. Residuals (difference between fiber and RTD measurements) for both fits are then plotted in the next two rows. Fit coefficients as well as the standard deviation of fit residuals are given in Table 2.
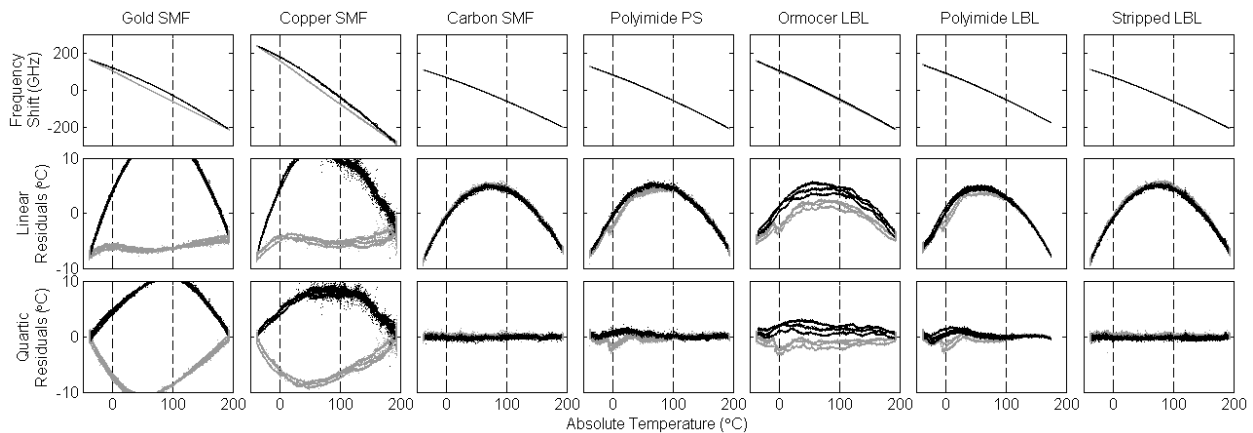
Figure 9. Temperature response of optical fiber with various coating types in the -40°C - 200°C range. Gray trace: up-ramps; black trace: down-ramps. Top row: Frequency shift against RTD temperature. Middle row: Residuals from linear fit. Bottom row: Residuals from quartic fit.

Bare glass fiber has a polynomial response to temperature, as seen from the parabolic shape of the linear fit residual for stripped LBL. A quartic fit captures the polynomial, resulting in residuals about zero. Looking across the various fiber types, the most uniform temperature response is obtained from stripped LBL as well as carbon coated SMF, as both of these have minimal quartic residuals. This indicates that both of these fibers would perform

very well as temperature sensors. Their linear and quartic coefficients are given in Table 2 below, for a 25°C baseline temperature. Quartic fits result in standard deviations well within 0.5°C.

Table 2. Linear and quartic coefficients for fiber sensors baselined at 25°C as well as the standard deviation of fit residuals.

Fiber	Linear (°C/GHz)	Quadratic (E^{-4} °C/GHz^2)	Cubic (E^{-6} °C/GHz^3)	Quartic (E^{-10} °C/GHz^4)	Standard deviation (°C)
Gold SMF	-0.657	-6.02	-19.75	-26.80	7.149
	-0.622				7.938
Copper SMF	-0.459	-3.69	-12.05	-13.52	5.922
	-0.435				6.718
Carbon SMF	-0.832	-8.82	-22.98	-32.60	0.262
	-0.748				4.392
Polyimide PS	-0.766	-5.93	-7.54	-4.87	0.558
	-0.691				4.242
Ormocer LBL	-0.670	-2.70	0.26	6.36	1.350
	-0.627				2.993
Polyimide LBL	-0.749	-6.25	-4.13	13.03	0.768
	-0.686				5.602
Stripped LBL	-0.811	-8.33	-19.07	-24.16	0.310
	-0.725				4.559

The gold- and copper-coated fibers exhibit large hysteresis, with the down-ramp exhibiting a larger deviation from a linear profile compared to the up-ramp. This can be seen from the linear residuals where the up-ramp residuals vary much less in magnitude than the down-ramp residuals, across the test temperature range. We postulate that this is due to a combination of CTE mismatch between glass and metal, as well as the non-specific bonding of the metal coating on the glass fiber, where the bond is a mechanical interaction (as opposed to chemical). The difference in behavior on the up- vs down- ramps indicates that separate fits on each of these segments would result in tighter tolerances in residuals. This is verified by fitting just the down-ramp of the metal and copper fiber measurements with a quartic fit. The residuals are plotted in Figure 10, and are shown to be similar to the residuals from stripped fiber. The stripped fiber residuals remain small for both ramps.

The polymer-coated fibers (polyimide and Ormocer), also exhibit some hysteresis, with the down ramp showing a smoother and more repeatable response. It is postulated that this is due to humidity effects on the polymer coating, as it is known that polymers may absorb moisture from air and swell in response, causing a humidity-dependent strain on the optical fiber. We believe that on the down-ramp, moisture has been baked out of the environment and therefore the polymer coated fiber exhibits a repeatable behavior. The sensor is then held at -40°C. The time spent at low temperatures allows the polymer to start absorbing moisture, causing it to exhibit drastic nonlinearities on the up-ramp. At temperatures above 100°C, the moisture is once again baked out of the polymer. There is minimal hysteresis in the 100°C-200°C range. Once again, this is verified by fitting just the down ramp of the polymer coated fiber measurements with a quartic fit. The residuals are plotted in Figure 10, and the down-ramp residuals are shown to be similar to the residuals from the stripped fiber.
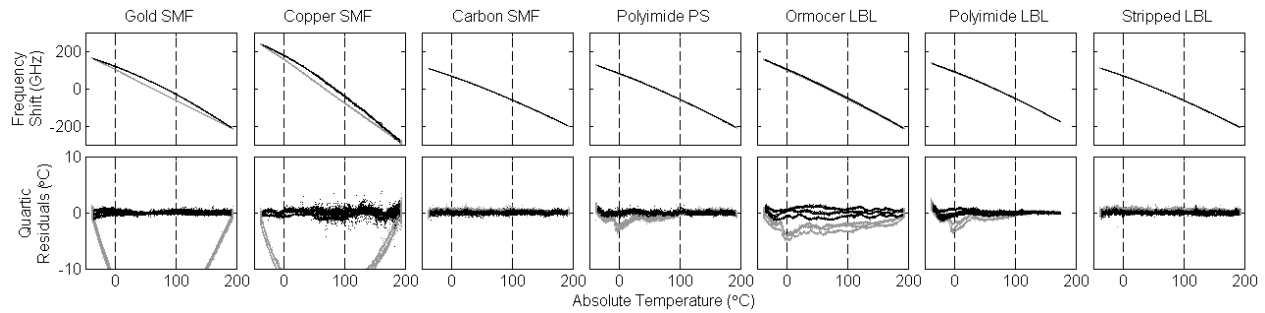
Figure 10. Temperature response of optical fiber with quartic fit carried out only on down-ramp data. Gray trace: up-ramps; black trace: down-ramps. Top row: Frequency shift against RTD temperature. Bottom row: Residuals from down-ramp quartic fit.

The humidity effects on the polymer-coated fiber were further investigated. Five humidity sensors (MK33 Mini, Innovative Sensor Technology) were added to the enclosure, and their readings were logged during a single -40°C to 200°C ramp. A plot of humidity against temperature is shown in Figure 11. It clearly shows that even though desiccant is used in the enclosure, moisture is still present in the environment, as humidity increases with decreasing temperature. This validates the association of the non-repeatability of the up-ramps of the polymer-coated fibers with humidity absorption.
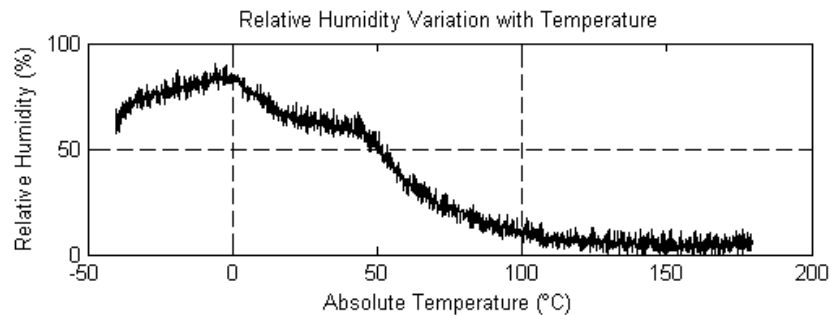
Figure 11. Relative humidity variation with temperature.

B. High Temperature Test

As the stripped fiber displayed better performance over the -40°C - 200°C range, a stripped fiber sensor configuration was selected for the high temperature long term test. For this test, the fiber frequency shift measurements were pegged to the 2nd thermocouple measurement of day 55 using a linear coefficient. Figure 12 shows the temperature profile across the furnace over 3 consecutive days (55, 56, 57). There is a 60°C variation across the furnace, from the entrance/exit to the central hottest region of the furnace. The fiber and thermocouple measurements are shown to match very well, proving the survivability of the fiber sensor for extended use at high temperatures. The truly distributed nature of the fiber optic temperature sensor has the added advantage of facilitating a more complete visualization of the temperature variation across the furnace.

American Institute of Aeronautics and Astronautics
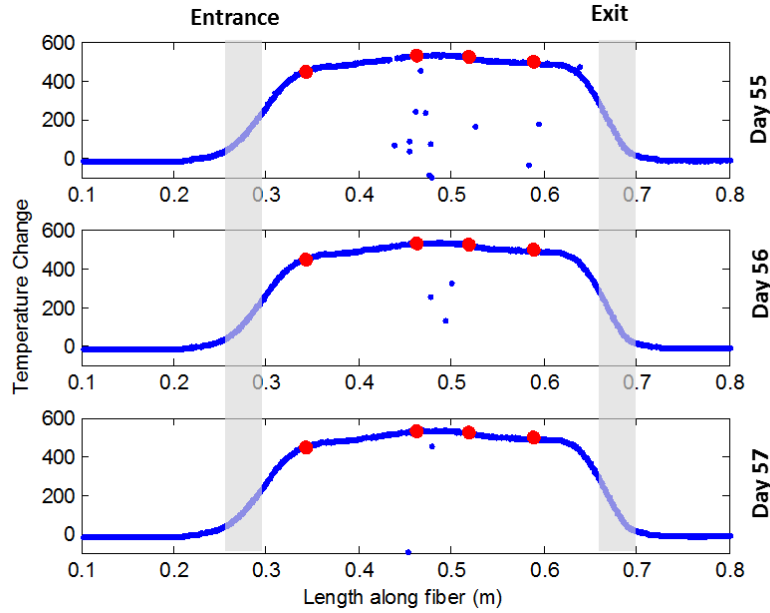
Figure 12. Temperature profile across the furnace over 3 consecutive days. Blue: Fiber measurements. Red: Thermocouple measurements.

It was determined that calibration coefficients from the -40°C - 200°C range cyclic test were not suitable for extrapolation to the larger temperature range. This meant that 4th order coefficients needed to be measured over a temperature range that encompasses the range of interest in order to be valid. Several sensors were placed into a different furnace to accomplish this calibration. Again, K-Type thermocouples were included at points along the sensors in the hot zone. The thermocouples were calibrated using a Fluke 9144 drywell facility.

The fiber sensors were taken through a thermal cycle and compared to the K-Type thermocouple measurements as shown in Figure 13. For each location a curve fit was obtained to relate the spectral shift to the applied temperature. The coefficients at each point were then averaged to provide a curve for the sensor. These coefficients can be seen in Table 3. The residuals at each of these points can be seen in Figure 14.

.

American Institute of Aeronautics and Astronautics
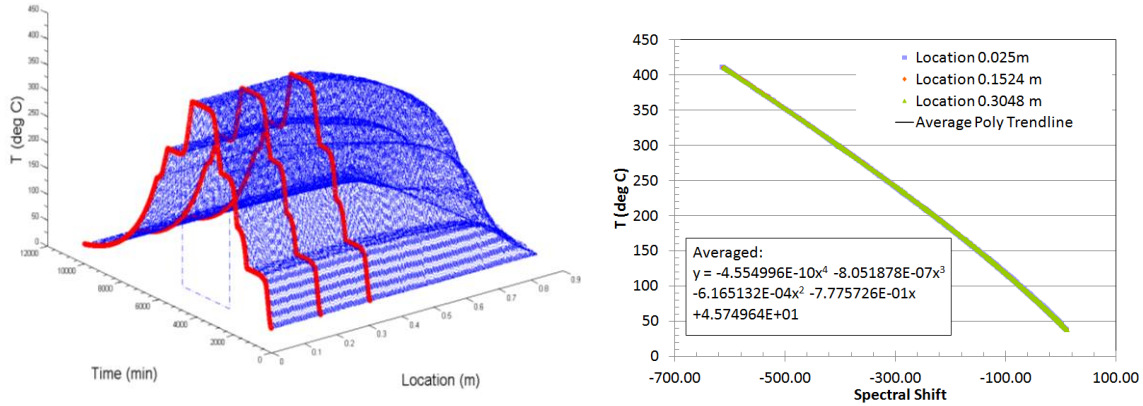
Figure 13. High temperature calibration test data. Left: Fiber data with thermocouple measurements overlaid at three locations. Right: The coefficients obtained from this comparison to relate spectral shift to temperature.
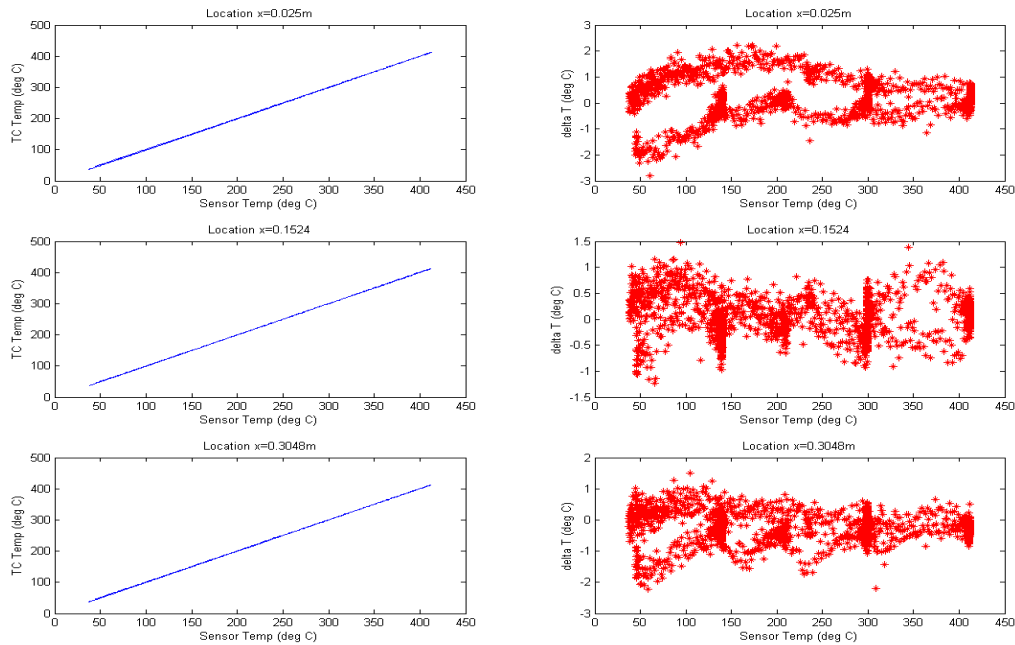
Figure 14. Residuals at each of the points using the previously obtained coefficients.

Table 3. Coefficients obtained from the high temperature calibration.

Location (m)	Constant	Linear (°C/GHz)	Quadratic (E^{-4} °C/GHz^2)	Cubic (E^{-7} °C/GHz^3)	Quartic (E^{-10} °C/GHz^4)	R²
0.025	45.797	-0.777	-6.385	-8.908	-5.360	0.9999593
0.153	45.477	-0.781	-6.226	-8.014	-4.455	0.9999874
0.306	45.975	-0.775	-5.884	-7.233	-3.850	0.9999808
Average	**45.496**	**-0.778**	**-6.165**	**-8.052**	**-4.555**	**0.9999758**

American Institute of Aeronautics and Astronautics

V. Conclusions

Both stripped LBL as well as carbon coated SMF display very repeatable performance throughout multiple cycles within the -40°C to 200°C range, with accuracies of +/-0.5°C. The performance of stripped LBL remains excellent in a packaged sensor configuration at higher temperatures. Polymer-coated fibers exhibit creep and humidity-related hysteresis while metal coated fibers show substantial hysteresis from slipping of the coating against the glass. These behaviors limit their accuracy as temperature sensors. The distributed nature of our measurement method coupled with good accuracy and survivability of fiber sensors provide clear advantages compared to single point thermocouples in terms of displaying localized temperature variations. Future work will be geared towards further sensor characterization including handling requirements, survivability and reliability of stripped sensors, as well as improved designs for better lifetime performance.

References

[1]Soller, B. J., Gifford, D. K., Wolfe, M., and Froggatt, M. E., "High Resolution Optical Frequency Domain Reflectometry for Characterization of Components and Assemblies," *Optics Express*, Vol. 13, Issue 2, 2005, pp. 666-674.

[2]Soller, B. J., Wolfe, M., and Froggatt, M. E., "Polarization Resolved Measurement of Rayleigh Backscatter in Fiber-Optic Components," *National Fiber Optic Engineers Conference*, 6 Mar. 2005, paper NWD3.

[3]Froggatt, M. E. and Moore, J., "High-Spatial-Resolution Distributed Strain Measurement in Optical Fiber with Rayleigh Scatter," *Applied Optics*, Vol. 37, Issue 10, 1998, pp. 1735-1740.

[4]Soller, B. J., Gifford, D. K., Wolfe, M. W., Froggatt, M. E., Yu, M. H., and Wysocki, P., F., "Measurement of Localized Heating in Fiber Optic Components with Millimeter Spatial Resolution," *Optical Fiber Communication Conference*, 5 Mar. 2006, paper OFN.

[5]Bos, J., Klein, J., Froggatt, M., Sanborn, E., and Gifford, D., "Fiber Optic Strain, Temperature and Shape Sensing via OFDR for Ground, Air and Space Applications," *Proc. SPIE 8876, Nanophotonics and Macrophotonics for Space Environments VII*, 24 Sept. 2013.

American Institute of Aeronautics and Astronautics